# Electromagnetic Precursors of Earthquakes Mediated by Ground Surface Plasma Wave, Part I: Stable Low-Noise Observation

Masafumi Fujii*

October 13, 2022

**Abstract**

The existence of precursors of earthquakes has been controversial; numerous trials of geodetic, seismological, geomagnetic, and geoelectric measurements have been performed extensively, and their results imply certain possibilities of detecting pre-seismic and co-seismic phenomena in the geoelectric measurements although the signals are subtle or vague. Other methods based on fundamentally different electromagnetic measurements could detect such precursors to a limited extent and their underlying mechanisms remain insufficiently elucidated. We show here that stable and clear detection of electromagnetic precursors of earthquakes is possible; an electromagnetic wave of a radio broadcast can be chosen as a tool and observed in an appropriate location. A large amount of electric charge carriers appear on the ground surface before earthquakes. They oscillate on coupling with the electromagnetic waves and manifest as a surface plasma wave on earth. The wave then propagates along the surface of the ground and occasionally re-radiates an electromagnetic wave at surface roughness. These phenomena can be detected as precursors of earthquakes. The optimal place for detecting such a surface plasma wave is a mountainous region or a coastline, where the radio wave propagates over and interacts with the surface plasma wave, particularly, where it traverses over a major fault zone. In Part I of this joint submission, we have addressed the observation of precursors, and the statistics and probability analysis on the relation between the precursors and earthquake occurrence, showing significantly high probabilities of earthquake prediction.

## Keypoints

- Stable detection of the electromagnetic precursors of earthquakes has been achieved by high-sensitivity low-noise observation.
- A super-narrowband notch (band-rejection) filter reduces intermodulation noises and allows the detection of earthquake precursors.
- Remarkable electromagnetic precursors were observed for the Fukushima offshore earthquake M7.4 on March 16, 2022, and many other events.

*Univ. of Toyama, 3190 Gofuku Toyama, Japan

# 1 Introduction

If earthquake prediction is the Holy Grail of seismology [1], electromagnetic measurement could be the first step of the approach. Electromagnetic signals are enhanced and transmitted to distant locations a few hours, days, or weeks before earthquakes. Researchers have tried to observe such geophysical electric and electromagnetic anomalies associated with earthquakes for more than 40 years [24, 28, 27, 12, 1, 13, 19, 18, 2]. Ground resistivity is reported to change at the time of earthquakes [24]. Low-frequency electromagnetic signals have been detected some days or hours before earthquakes [28, 27]. However, the observation of such anomalies has been extremely difficult because the equipment may become extensive, the signals are too subtle or vague, affected significantly by geographical, atmospheric, and ionospheric conditions, and often disturbed by various environmental and artificial noises. Some methods have been successful in an electromagnetically quiet environment [28], while these are ineffective elsewhere if artificial noises exceed signals.

From a theoretical point of view, the mechanism of anomalous radio wave propagation can be explained reasonably by the ground surface plasma wave appearing on the surface of the earth [8, 10]. Despite the controversies regarding the origin of the electric charges or charge carriers, they are certainly generated in various forms by tectonic activity and stress inside the earth's crust depending on the types of the rocks and their underground environment, particularly the existence of underground water [4, 20, 26, 3]. Studies have experimentally shown that positive charge carriers come out from the peroxy bond in oxidized minerals when rocks are subjected to tectonic deviatoric stresses even without fracture of rocks [5, 6, 2]. This is one of the plausible mechanisms similar to, but different from the piezoelectric effects of silicate minerals. These facts explain the possibility of electrostatic or mobile charges appearing on the earth's surface associated with co-seismic or pre-seismic, or occasionally aseismic, crustal activities. In general, if some electrical charges exist on a surface, either electrically positive or negative, the charges can oscillate with the external electric field. This is equivalent to the well-known surface plasmon in optics induced by light on metal surfaces [17, 22, 23, 9]. We assume that a sufficient amount of charge carriers exist on the earth's surface, and an oscillation of the surface charge carriers is induced, i.e., as a terrestrial ground surface plasmon, by radio wave propagation over the ground [8, 10],

The charge density has been estimated experimentally by applying stress to a gabbro tile [25], which shows that a large amount of surface charge carriers are involved before earthquakes and that the terrestrial ground surface plasmon can be induced. Such mobile charge carriers of the same sign diffuse by electrical repulsive forces. Thus, in a mountainous region, the charge carriers move to sharp wedges or peaks of mountains and the outstanding vertical electric field is induced there. In contrast, when the charge carriers appear near a coastline or in the ocean, they do not accumulate but diffuse to recombine with charges of the opposite sign before disappearing; cliffs and/or beaches on a coastline may lead to a different appearance and polarization of the radio wave anomaly as compared to mountainous regions. Therefore, studying the mechanism of radio wave propagation that can carry precursory signals of earthquakes is particularly important.

Detection of the surface plasma wave on earth is closely related to the geological measurement of geoelectric potential or ground resistivity that has long been studied for earthquake prediction. Ground resistivity shows abrupt changes coincidentally at the time of earthquakes [24]. The change in the ground resistivity is observed at a considerably large distance from the epicenter even at 1,000 km away, and clear relation is seen between the magnitude of the event and the reachable distance of the phenomena [24]. Some geoelectric signals have been obtained before earthquakes [28, 27] while measuring low-frequency electromagnetic fields or geopotentials by placing large dipole antennas of 100 m to 10 km under the ground. If electrical charges

are generated in the ground by seismic activity and appear on the surface, the moving charge and their fluctuation may cause changes in the electrical property of the earth and may radiate electromagnetic fields. Those phenomena are sometimes highly ambiguous and disturbed by artificial noises. However, there exist some intriguing properties in the ground resistivity and geopotential that match the electromagnetic wave measurement results. The ground resistivity changes because of changes in the electronic state of rocks under tectonic stresses. From this perspective, the ground surface wave can be detected reasonably at such a distance from epicenters; moreover, the larger the earthquake, the greater and clearer the expected precursory signals.

This paper addresses a high sensitivity and low noise observation of anomalous precursory signals possibly related to earthquakes carried by the very high frequency (VHF) radio wave. Radio wave measurements are essentially highly sensitive because they detect signals by mixing with highly accurate reference signals in frequency and phase, employing sharp filters to pick up only necessary signals, and enabling the demodulation of weak signals at the microwatt level. Moreover, they cover a wide area of hundreds of kilometers. To further improve the clearness of the electromagnetic precursors that are extremely subtle and random, a notch filter, or a band-rejection filter, having a super-narrow bandwidth in the order of 1 MHz has been implemented in our observation systems. The notch filter reduces the noise floor significantly and allows the detection of the precursory signals hidden behind noises.

Our recent observation of the electromagnetic waves shows the detection of clear signals before large earthquakes. The observation has been performed in Toyama city on the west side of Japan near the coast opposite the Pacific Ocean, and in Iwata city facing the Pacific Ocean, each located on the opposite side of Japan ' s main island. It is particularly noteworthy that typical precursory signals have been observed for the geometries where radio waves propagate over large fault zones such as the Median Tectonic Line and Shizuoka-Itoigawa Tectonic Line. Electrical charges may move differently through fault zones as compared to the middle of a crust [6, 7]. On March 16, 2022, a large earthquake occurred at Fukushima offshore of the Pacific Ocean while our observation system was in operation. Since some days before the event, we had been detecting large electromagnetic precursors in the radio wave signals. The measured precursory signals have been carefully compared with other possible noise sources of meteorological and other environmental conditions. In the last section of this paper, statistical analysis of the precursors is discussed. Probabilities regarding the success rate of earthquake prediction and the predicted rate of earthquakes are analyzed.

This is a joint submission of two papers. In Part II accompanying this paper, we have validated the phenomena of precursory radiation of electromagnetic waves by numerical analyses with extensive and accurate geographical digital landform models. The interactions between the surface plasma waves and radio waves are analyzed for the actual locations where precursory signals have been detected in our observation. Rapidly communicating the methods of observation of electromagnetic precursors is crucial in the series of large earthquakes expected in the close future.

## 2 Method of High Sensitivity Radio Wave Observation

### 2.1 Geography of the Radio Wave Observation

We observe radio waves at three locations from different broadcast stations as shown in Fig. 1. The Iwata observation station (E137° 49'20", N34° 39'20", altitude 4 m) is in Iwata city on the Pacific coastline, which receives two radio waves: one at 79.2 MHz of power 1 kW, horizontal polarization from a broadcast station in Shizuoka city (E138° 27'56", N34° 58'27", alt. 300 m),

and the other at 78.9 MHz, 3 kW, horizontal polarization from a broadcast station in Tsu city (E136° 26'01", N34° 43'57", alt. 320 m). The Toyama observation station (E137° 11'13", N36° 41'38", alt. 30 m) is in Toyama city and the antennas are placed on top of a building, which receives a radio wave at 82.3 MHz 1 kW, horizontal polarization from a broadcast station in Niigata city (E138° 48'30", N37° 42'24", alt. 600 m), on the west side of Japan. The Yatsuo observation station (E137° 07'51", N36° 37'10", alt. 30 m) is not shown in Fig. 1 and is located in the Yatsuo district which is 10 km south of Toyama observation station and receives the same radio wave as Toyama station; measurement at these nearby stations helps to distinguish artificial noises in the observed data. It is noteworthy that those broadcast stations and observation stations are located such that the radio waves propagate over the large fault zones of the Median Tectonic Line and Shizuoka-Itoigawa Tectonic Line. These geometric arrangements resulted coincidentally, as discussed later when we studied the datasets that include anomalous precursory signals; the other datasets observed at locations with radio waves that do not propagate over the tectonic lines do not convey precursory signals.

## 2.2 Noise Reduction by Super-Narrowband Notch Filter and Measurement System

The radio wave measurement system is composed of standard Yagi antennas of 5 elements in horizontal polarization and digital radio receivers AOR AR5001D and/or AR2300, which are controlled by PCs or single-board computers. The radio wave is measured every 10 s at Toyama and Yatsuo stations, and every 20 s at Iwata station. For the stable detection of the precursors of earthquakes, elaborate noise reduction is essential in the measurement system. Super-narrowband notch (band-rejection) filters [11] are inserted between the antenna and the receiver to reduce unwanted radio waves from nearby broadcast stations by more than 20 dB from typically −50 dBm signal level down to −70 dBm, etc., allowing clear uninterrupted observation even in urban areas.

The frequency characteristics of the super-narrowband notch filter used for the Toyama observation station is shown in Fig. 2 (a). The filter attenuates the radio wave signals from nearby stations each by −25 dB and the rejection bandwidth is as narrow as approximately 1 MHz. Because the target signal from the Niigata broadcast station at 82.3 MHz is very close to the unwanted signal at 82.7 MHz, the target signal is also attenuated by approximately −11 dB; this may unfortunately degrade the necessary radio wave signal. However, the third-order intermodulation caused in the amplifying circuit of most receivers would have worse effects, which has been reduced by the filters by more than −30 dB. This leads to the reduction of the noise floor under −90 to −100 dBm as shown in Fig. 2 (d). The effect of the filter is recognized when the filter is removed for maintenance on March 9, 2022, from 12:00 to 17:00, and the noise floor rose by 30 dB to 40 dB depending on the frequency. Reduction of the third-order intermodulation noise is thus found critical and given a higher priority than the slight loss of the necessary signal; otherwise, precursors are weak and hidden behind noises.

The super-narrowband notch filter is composed of a series capacitor of several pico-farads and a high-quality-factor (low-loss) inductance of approximately 1 nH. The inductance is established by a short-circuited low-loss 12D-FB coaxial cable of length 60 cm to 70 cm, determined according to the frequency to be rejected, and has a quality-factor of approximately 25 to 30 at the VHF band. The circuit is shown in Fig. 2 (b) for a unit structure; for its use in actual observation, a necessary number of the unit structures are cascaded as in Fig. 2 (c). It is noted that usual commercial products of inductors are not applicable due to their much larger loss and lower quality factor.

Similar notch filters are used in all the observation systems to attenuate unwanted radio wave signals and reduce the noise floor. Heading into a rural unpopulated district to search

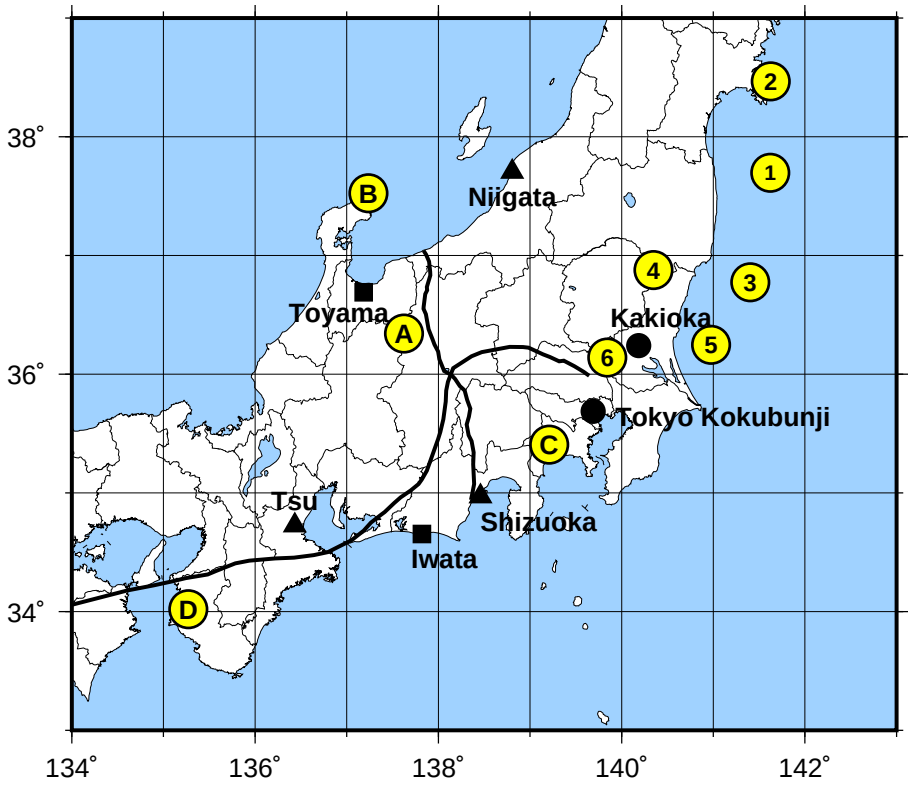


Figure 1: Locations of the radio wave broadcast stations (▲), radio wave observation stations (■), and meteorological and ionospheric observation facilities of JMA and NICT (●) in the middle part of Japan's main island. Numbers inside a circle (○) denote the epicenter of the earthquakes (EQ.) discussed in the following part of this paper, i.e., EQ.1: Fukushima offshore $M7.4$ on March 16, 2022, EQ.2: Miyagi offshore $M6.9$ on March 20, 2021, EQ.3: Ibaraki offshore $M6.0$ on May 22, 2022, EQ.4: Ibaraki north inland $M5.4$ on April 19, 2022, EQ.5: Ibaraki offshore $M5.3$ on May 29, 2022, and EQ.6: Ibaraki south inland $M4.8$ on May 5, 2022, A to D inside a circle (○) denote the approximate area of other earthquakes detected near the radio wave observation stations, i.e., A: Gifu Hida district, B: Ishikawa Noto district / Noto peninsula, C: Kanagawa west area, and D: Wakayama north area / Kii channel. Thick solid lines are the Median Tectonic Line (west to east) and Shizuoka-Itoigawa Tectonic Line (south to north), the major fault zones in Japan, respectively.

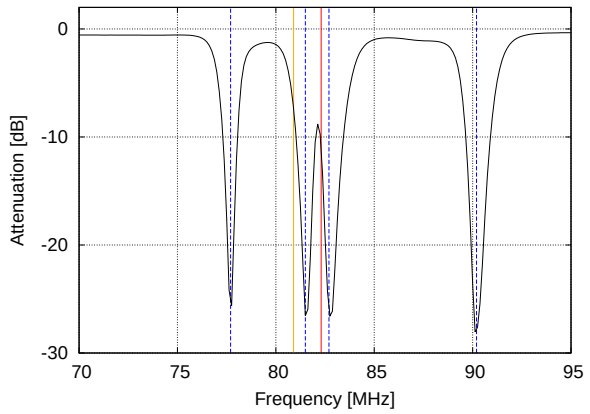


(a)

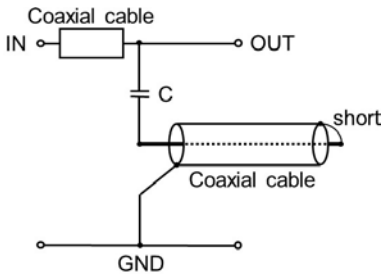


(b)

(c)

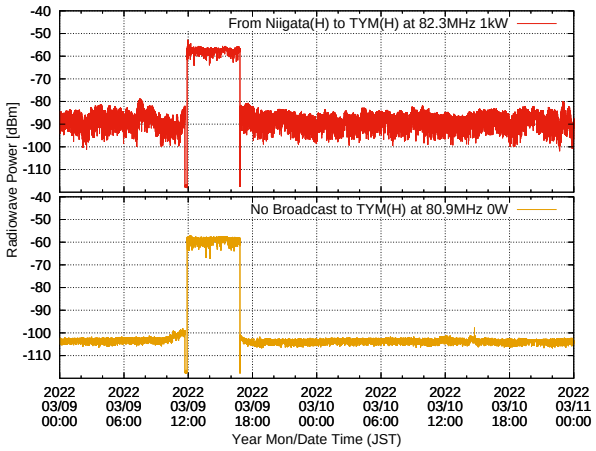


(d)

Figure 2: The super-narrowband notch filter implemented in the observation equipment. (a) Frequency characteristics of the whole filter. Blue dotted lines are the frequencies to be rejected i.e., 77.7 MHz, 81.5 MHz, 82.7 MHz, and 90.2 MHz for the Toyama station, and the orange and red solid lines are the target frequencies to be observed at 80.9 MHz and 82.3 MHz, respectively. (b) Unit circuit of the notch filter. (c) The appearance of the whole filter. A total of 8 units are cascaded to reject 4 frequencies. The coaxial cables are rolled to fit in a 25 cm × 30 cm × 10 cm-high box. (d) Noise reduction effect of the filter; the filter was removed for maintenance on March 9th from 12:00 to 17:00, i.e., the upper part of the step, otherwise inserted. The height of the step is, therefore, the level of the achieved noise reduction.

for a quiet environment is not necessary if such a filter is used in the observation system. In addition, coaxial cables connecting antennas and receivers are loaded with numerous ferrite cores to reduce the common-mode noise. The target broadcast stations are extensively chosen in such a way that their radio signals are significantly weak but very close to the limit of detection. The system needs to be run for a certain period and a radio wave that can carry anomalies under the critical propagation conditions should be sought.

Table 1: List of the earthquakes focused in this paper. Magnitude $M$ is of JMA. The observed maximum seismic intensity of the Japan scale (Max SI) is also shown.

| EQ. | Epicenter | $M$ | Date | Time (JST) | depth | Max SI |
|---|---|---|---|---|---|---|
| 1 | Fukushima offshore | 7.4 | March 16, 2022 | 23:36:32.6 | 57 km | 6+ |
| 2 | Miyagi offshore | 6.9 | March 20, 2021 | 18:09:44.8 | 59 km | 5+ |
| 3 | Ibaraki offshore | 6.0 | May 22, 2022 | 12:24:11.3 | 5 km | 5− |
| 4 | Ibaraki north inland | 5.4 | April 19, 2022 | 8:16:00.3 | 93 km | 5− |
| 5 | Ibaraki offshore | 5.3 | May 29, 2022 | 15:55:22.5 | 44 km | 4 |
| 6 | Ibaraki south inland | 4.8 | May 5, 2022 | 18:42:02.1 | 52 km | 4 |

# 3 Observed Precursors of Earthquakes

## 3.1 Earthquakes Focused in This Paper

We have been detecting electromagnetic precursors of earthquakes steadily since the observation started approximately 5 years ago. Table 1 is the list of recent earthquakes that we focus on in this paper and these are numbered in the order of their magnitude.

The largest event is EQ.1 in Table 1, Fukushima offshore $M7.4$ earthquake on March 16, 2022. The local seismic intensity detected in the Tonankai region, where the Iwata observation station locates, was 4, and that in the northwest region (or Hokuriku region), where the Toyama observation station locates, was 5−. Precursory signals of this event have been observed several days before, and a large and clear anomalous signal was observed one day before the main shock. These signals will be discussed later. Another earthquake EQ.2 Miyagi offshore $M6.9$ had occurred on March 20, 2021, a year before EQ.1 at the same location and depth, with the same level of magnitude. For this event, the local seismic intensity observed in the region of the Iwata observation station and that in the region of the Toyama observation station were both 4. The anomalous signals observed before this event will be compared and discussed in detail with those of EQ.1 Fukushima offshore $M7.4$.

Further examples of the radio wave signals before recent smaller earthquakes would provide some clearer insight into the probability of successful detection of the precursors. An earthquake of a smaller size, EQ.3, Ibaraki offshore $M6.0$ occurred on May 22, 2022, two months after EQ1 at a similar location but in a shallower region. A smaller event, EQ.4, also occurred at a similar location but in a deeper region as compared to other earthquakes, at Ibaraki north $M5.4$ earthquake on Apr. 19, 2022. An even smaller event of EQ.5, Ibaraki offshore $M5.3$ earthquake occurred shortly afterward on May 29, 2022, at the south of the Fukushima offshore $M7.4$ epicenter. The last example is the event that occurred inland, EQ.6, Ibaraki south $M4.8$ earthquake on May 5, 2022. We have detected precursory signals for many events during our observation period and some of the most particular events have been described in this paper. These signals are clearer as the magnitudes become larger, which will be discussed later in detail.

In Figs. 3 (a) to (f), the distribution of the seismic intensity of Japan scale 1 to 4, 5−, 5+, 6−, 6+, and 7 is shown for each earthquake. These maps have been publicized by the Japan Meteorological Agency (JMA) in their seismic intensity database. For EQ.1 Fukushima offshore $M7.4$ event, the mechanical geodesic shock spreads over 1,000 km as in Fig. 3 (a). Hence, despite their independent mechanisms, electric charge carriers may spread over farther distances comparable to that of mechanical shocks. Electromagnetic precursors have been detected at the distances as far as those of earthquakes exemplified in this paper For EQ.2 Miyagi offshore $M6.9$ event, the shock reached the location of the Iwata observation station and the Toyama observation station. Possible precursory signals are clearly observed in those radio wave data. For the other

earthquake examples with magnitudes below 6.0, the mechanical shock of the earthquake was less than 1 on the intensity scale at the observation stations. It is of particular interest to estimate the possible reaching distance of the electric charge carriers even if the mechanical shocks are not reachable. This can be considered by comparing the smaller earthquakes of Figs. 3 (c) to (f) with the following radio wave signals.

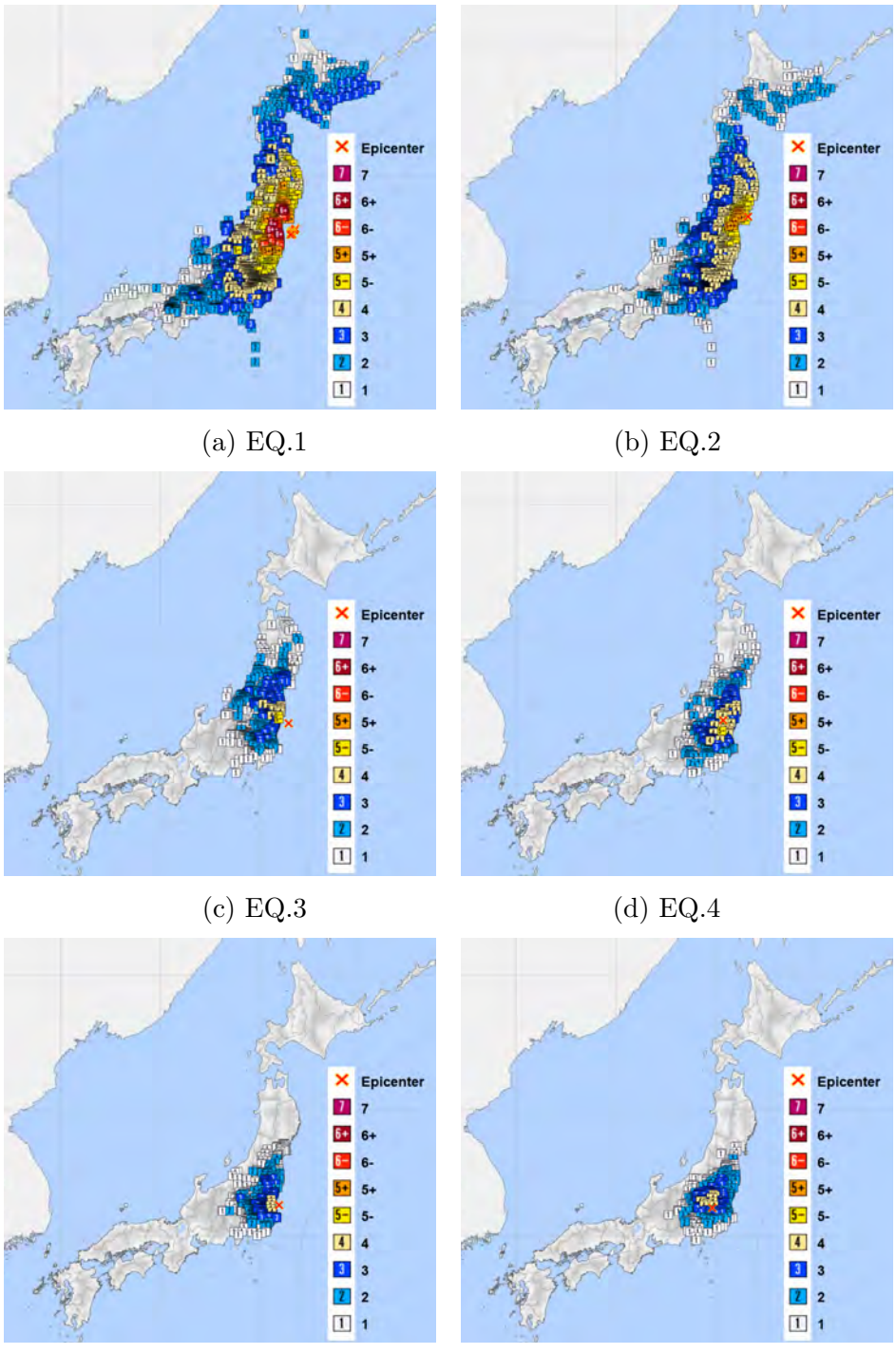


(a) EQ.1 (b) EQ.2

(c) EQ.3 (d) EQ.4

(e) EQ.5 (f) EQ.6

Figure 3: Map of Japan showing the seismic intensity distribution of earthquakes EQ.1 to EQ.6 in Table 1. Color indices are obtained from the Japan seismic intensity scale publicized by the Japan Meteorological Agency (JMA).

### 3.2 Observed Electromagnetic Precursors of Earthquakes

Observed radio wave signals are shown in Figs. 4 to 13 together with other environmental data: local temperature and precipitation, ionogram of the ionospheric E-layer in Kokubunji, geomagnetic field in Kakioka, the magnitude of the earthquake, local seismic intensity of Japan scale detected in the region of the observation stations, and epicentral district names. This information is publicized officially by JMA and the National Institute of Communication Technologies (NICT), Japan. The signal level at 80.9 MHz is monitored, at which frequency no broadcast wave is assigned; this helps to distinguish noises generated from other wideband electromagnetic sources. The broadcast station and the observation station are noted in each radio wave plot with the frequency and the power of the wave. The notation '(H)' shows that the transmitting or receiving antenna is horizontally polarized. We also measure vertically polarized radio waves, although this is not addressed in this paper but will be discussed in our succeeding paper.

#### 3.2.1 Large Earthquakes and Their Precursors

In Fig. 4, clear precursors of sudden increase and decrease are observed during a short time of several hours as highlighted by the yellow background before the main shock of EQ.1 Fukushima offshore $M7.4$ earthquake indicated by a star. The signal level at 80.9 MHz stays the same, indicating that the precursors are not from any other wideband noises. Moreover, the weather and the ionogram do not show even small changes, and hence the precursors did not originate from the influence of the weather or the ionospheric E-layers. The geomagnetic field does not show any changes either, around March 16, 2022, suggesting that the anomalous signal was not caused by solar turbulences. In Fig. 4, smaller signal variations are seen from March 11 to March 14, 2022, in the data from Tsu at 78.9 MHz. This could be due partly to the smaller earthquakes around March 11 to March 15, 2022, but could have been influenced also by the crustal stresses that caused the event of Fukushima offshore $M7.4$ on March 16, 2022.

In Fig. 5, precursors are also seen at the Toyama and Yatsuo observation stations in the west of Japan as highlighted by yellow backgrounds, before EQ.1 Fukushima offshore $M7.4$. The weather conditions and the 80.9 MHz signal do not change near the Toyama observation station on the day of the event. The time variation of the radio wave power behaves similarly to those of Iwata as in Fig. 4. Smaller earthquakes occurred in Ishikawa Noto, Gifu Hida (see areas B and A, respectively, in Fig. 1) before EQ.1, and smaller precursory signals are also seen slightly before the smaller earthquakes.

In EQ.2 Miyagi offshore $M6.9$, a large variation is seen in Fig. 6 in the 78.9 MHz data from Tsu broadcast station approximately 2 days before the event. Other data of precipitation, temperature, and ionograms show little change simultaneously with the radio wave signals, suggesting almost no possibility of the influences from the meteorological or ionospheric conditions; the 80.9 MHz data remains the same, i.e., there is no influence of wideband noises from other sources. In the same figure, relatively large earthquakes occurred in Wakayama north (see area D in Fig. 1), on March 15, 2021, at 0:25:59.3 JST with $M4.6$ depth 4 km; for this event, small precursors were observed on March 12, 2021. It is noteworthy that in Fig. 6, the variation in the signal of 78.9 MHz and 79.2 MHz data on March 15, 2021, at around 1:00 to 4:00 JST, is not an anomaly but an artificial noise when the radio wave is stopped for regular maintenance of the broadcast stations early on Monday morning. A small signal variation is seen again on March 16, 2021, in the same data; a few hours later, Ibaraki south earthquake $M4.9$ occurred (not shown in Fig. 1; Ibaraki is on the Pacific side of Japan) on March 16, 2021, at 4:56:18.1 JST at a depth of 54 km, which may have caused the precursor. The geomagnetic field show some ripples on March 20, 2021, as shown in Fig. 6, which might have some unknown relations to the earthquake on the same day; however, the electromagnetic precursors do not coincide with the

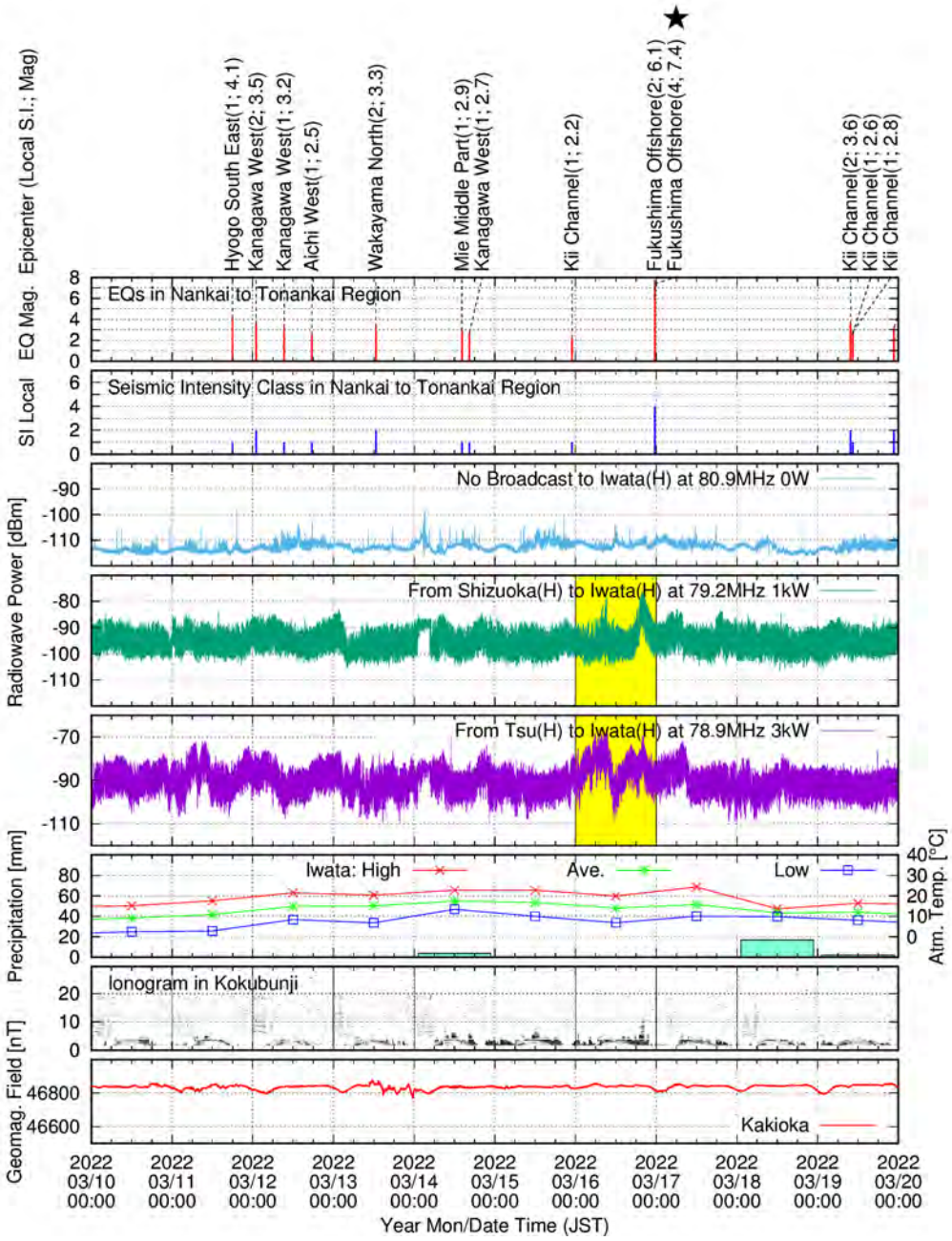


Figure 4: Observed radio wave power (dBm) at Iwata observation station on the Pacific side of Japan around EQ.1 earthquake in March 2022, together with environmental data observed by national institutes. The main shock of EQ.1 is marked by a star.

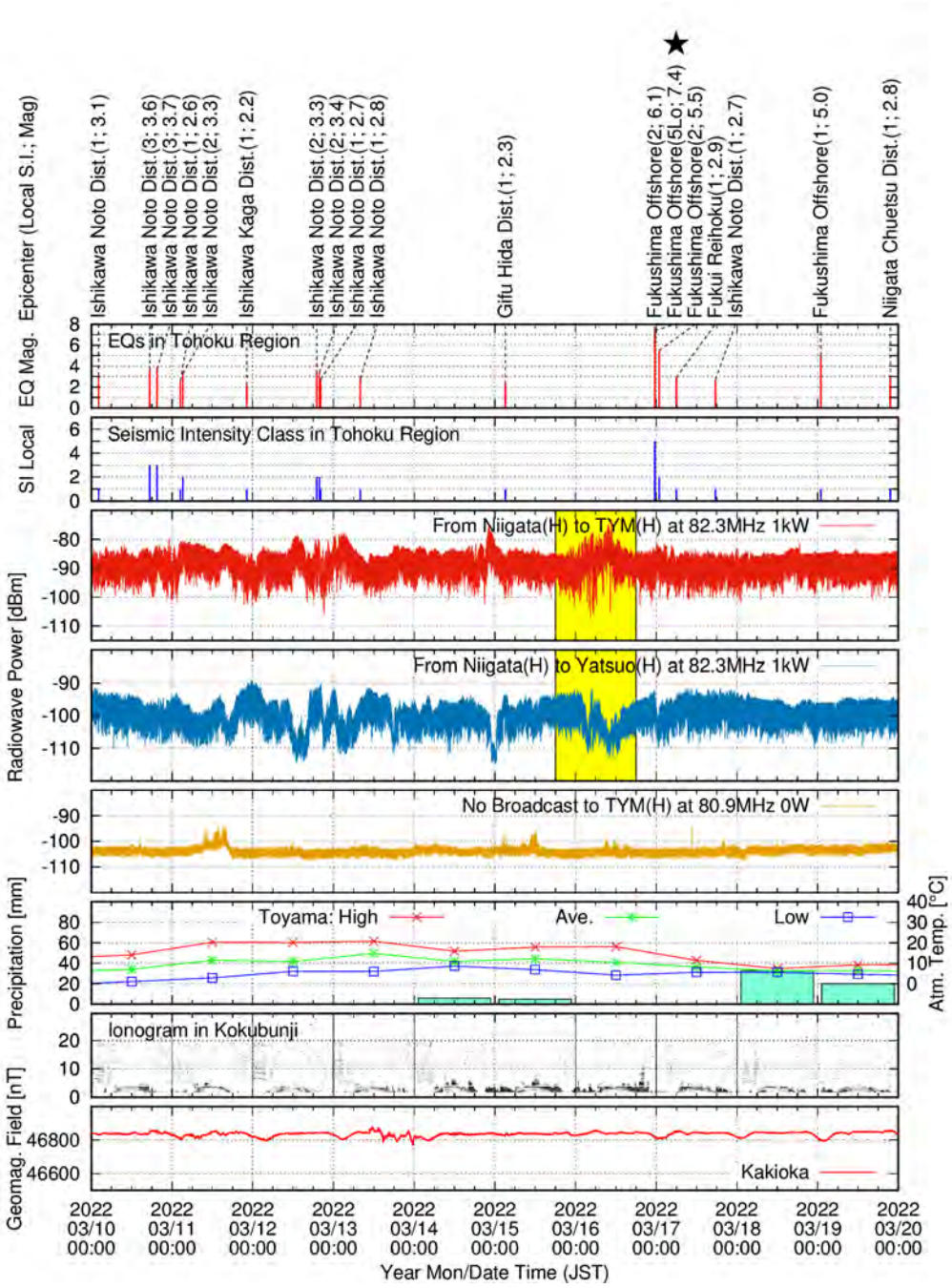


Figure 5: Observed radio wave power (dBm) at Toyama (TYM) and Yatsuo observation stations on the west side of Japan around EQ.1 earthquake in March 2022, together with environmental data observed by national institutes. The main shock of EQ.1 is marked by a star.

geomagnetic field ripples.

In Fig. 7, precursors are seen but are rather ambiguous at the Toyama and Yatsuo observation stations as highlighted by yellow backgrounds before EQ.2. The main reason for the ambiguity of the precursors would be because the magnitude is smaller and the epicenter is further for EQ.2 from the Toyama and Yatsuo observation stations as compared to EQ.1. In the same figure, there is no obvious evidence that the meteorological, ionospheric, and geomagnetic field conditions generated the precursory signals, which is also the case for the precursors that we have detected so far.

It is also interesting to note in Figs. 5 and 7 that the variations of the radio wave power at 82.3 MHz observed in Toyama (TYM, red line) and those in Yatsuo (blue line) are mostly opposite considering its increase or decrease; these observation stations are only 10 km apart, for which an opposite behavior of the received power cannot be explained by the simple meteorological radio ducting or any other influence from ionospheric layers. When the radio wave power is stronger in Toyama, it is weaker in Yatsuo, implying that the radio wave radiated from Niigata at 82.3 MHz, and is focused slightly northward to the direction toward Toyama than toward Yatsuo. Such beam-steering-like propagation of a radio wave is explained by the steep focusing effect [10] of the terrestrial surface plasmon on mountain ranges, which can depend on the geography, plasma frequency, and thus the strength of the seismic activity [9, 10]. The observation station in Toyama (TYM) is on the west side of Japan island, more than 300 km away from the epicenters on the Pacific side. The crustal structure in this district is complicated and consists of intricate large faults. Considering those facts and possible mechanisms that relate to the propagation of charges through lithospheric structures and faults as suggested by the ground resistivity measurement [24], it is inferred that the precursors may travel over a long distance to reach the other side of the island.

### 3.2.2 Comparison of the Precursors of Large Earthquakes

It is noteworthy that the precursors in Figs. 4 to 7 have similarity and simultaneity, despite the observation stations being more than 200 km apart; those precursors are plotted together and compared in detail in Figs. 8 and 9. Note the time of the two observation systems is synchronized by the internet time server and the time difference is less than a second.

In Fig. 8 (a), the precursors appear simultaneously in the morning of March 16, 2022, in Toyama (TYM) 82.3 MHz and in Iwata 78.9 MHz data. Intense oscillations (with yellow highlight) are observed with a period of 1 to 2 h. Those are typical precursors so far observed before large earthquakes. More detail of the signal exhibits some differences as shown in Fig. 8 (b) on the day of the earthquake between the signal in Toyama (TYM) 82.3 MHz and that in Iwata 78.9 MHz, i.e., some sudden drops are seen in Toyama (TYM) 82.3 MHz, while they are not seen in Iwata 78.9 MHz. If the radio wave anomalies occur solely in the atmosphere near the epicenter, they must appear simultaneously and identically because the radio wave propagates at the speed of light. The time difference of the anomaly could be the evidence that the anomaly occurs not only in the atmosphere but is mediated by other mechanisms such as those on the ground surface and/or underground geology.

The simultaneity of the precursors between Toyama (TYM) 82.3 MHz and Iwata 78.9 MHz for EQ.1 Fukushima offshore $M7.4$ in Fig. 8 (a) is slightly better than the case for EQ.2 Miyagi offshore M6.9 in Fig. 9 as mentioned earlier. This could be because the magnitude is larger and the epicenter is closer for EQ.1, but there might be other unknown reasons regarding the underground faults and crusts.

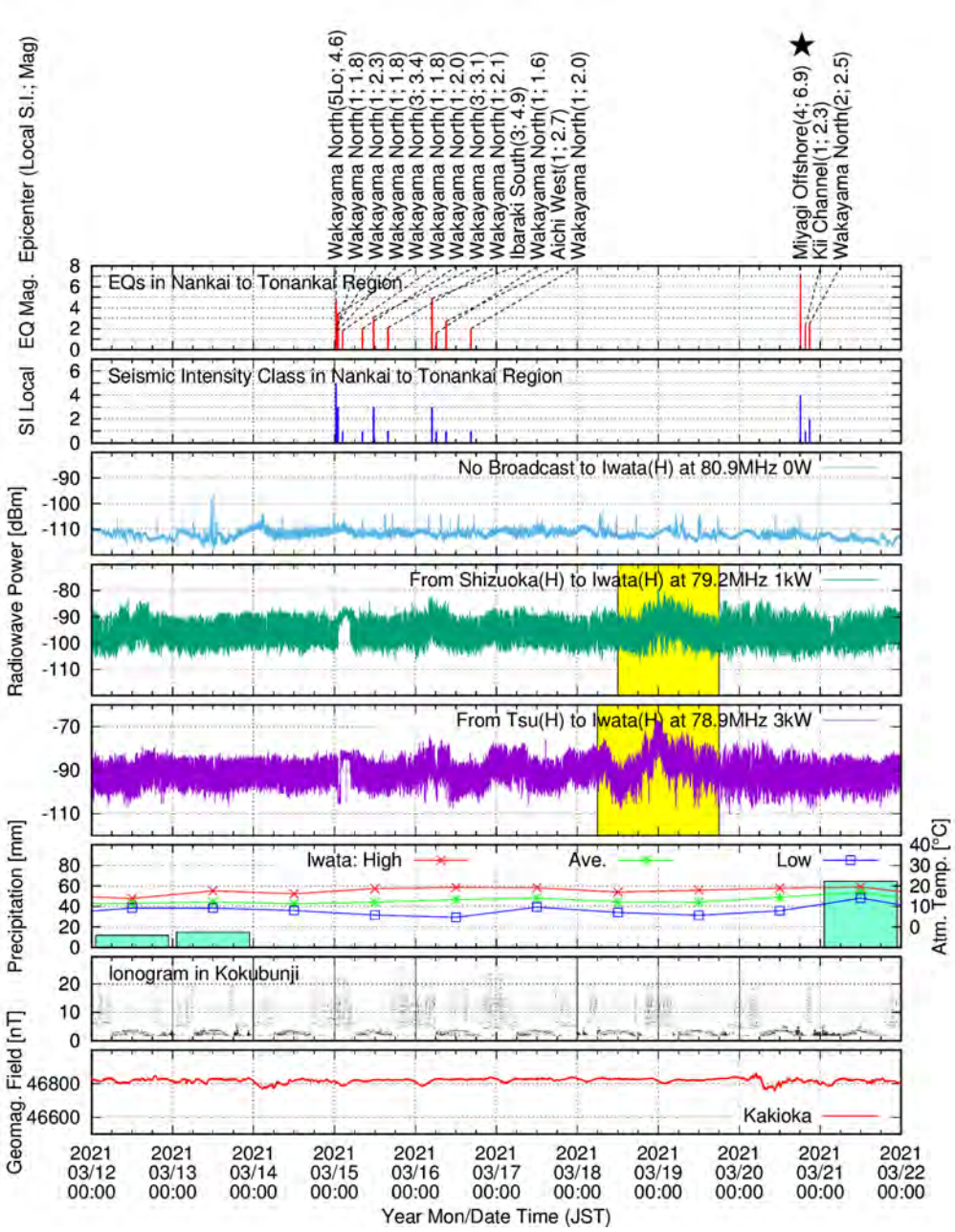


Figure 6: Observed radio wave power (dBm) at Iwata observation station on the Pacific side of Japan around EQ.2 earthquake in March 2021, together with environmental data observed by national institutes. The main shock of EQ.2 is marked by a star.

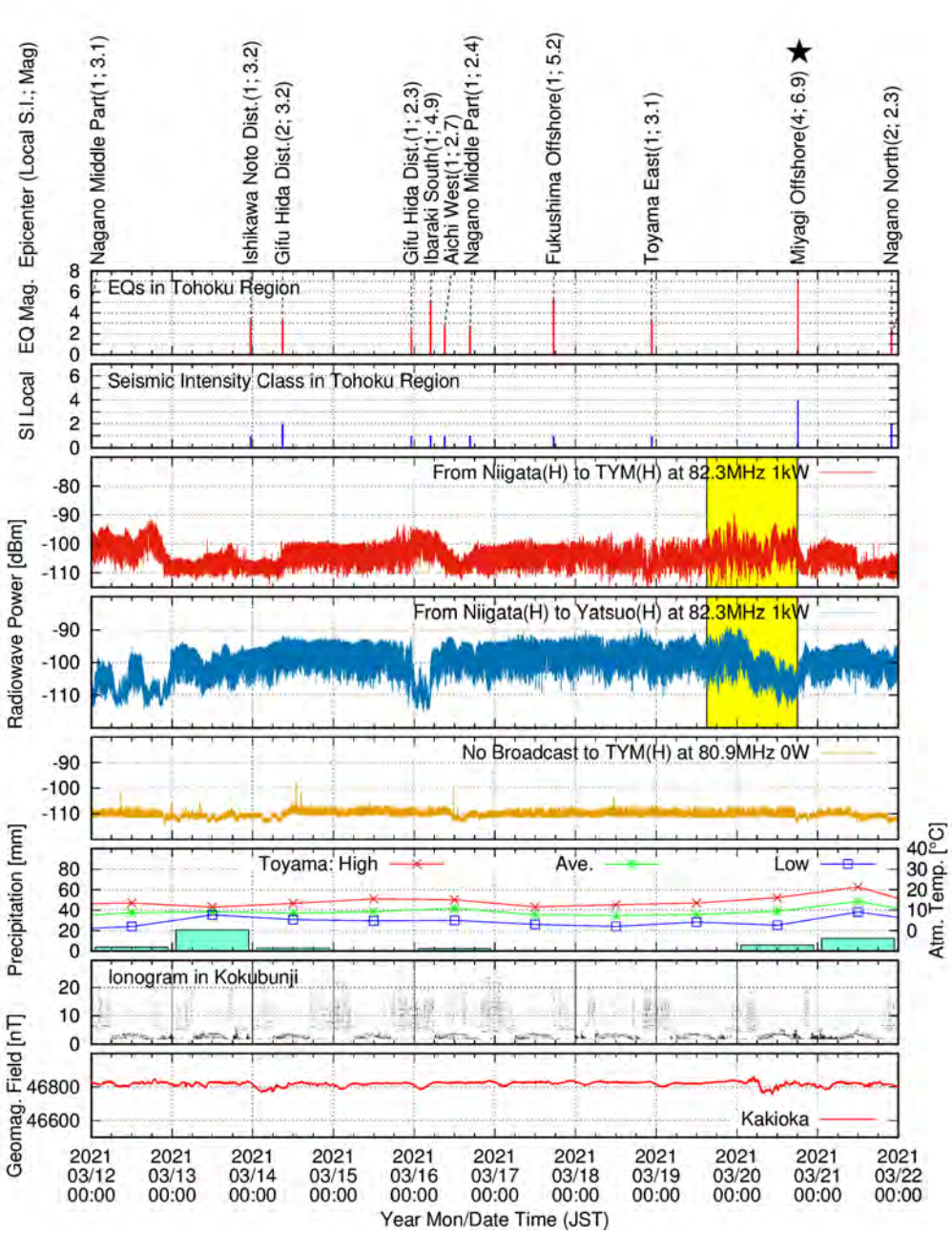


Figure 7: Observed radio wave power (dBm) at Toyama (TYM) and Yatsuo observation stations on the west side of Japan around EQ.2 earthquake in March 2021, together with environmental data observed by national institutes. The main shock of EQ.2 is marked by a star.

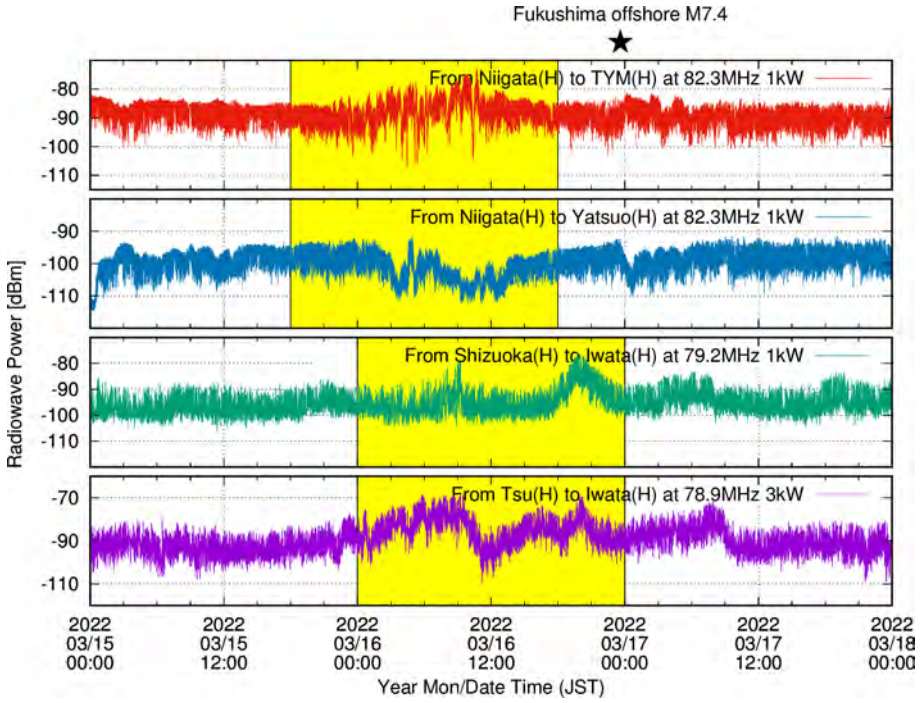


(a)

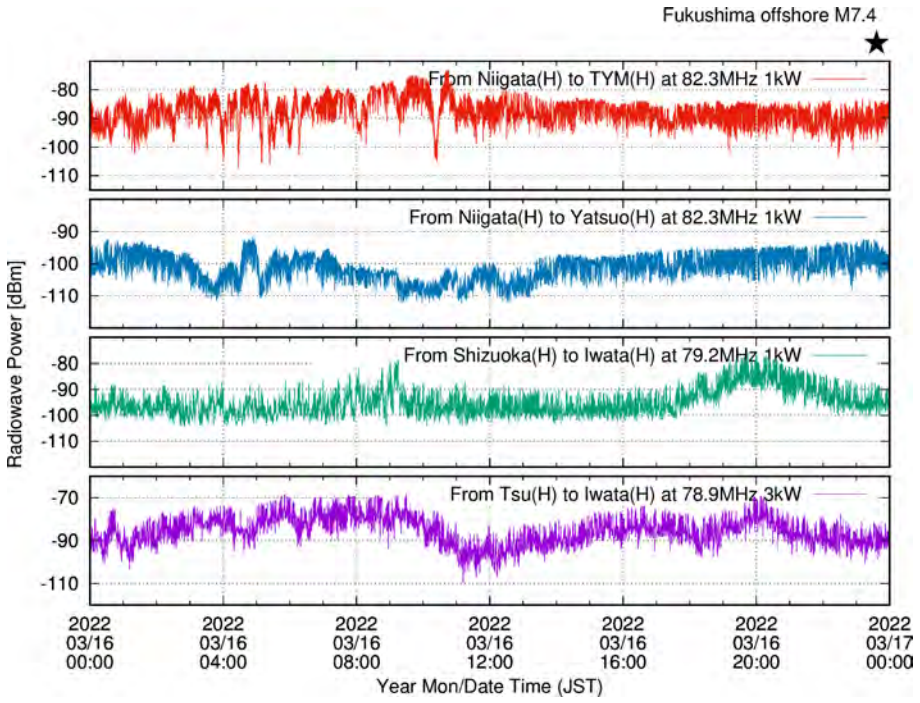


(b)

Figure 8: Expansion and comparison of the precursory signals observed in Iwata, Toyama, and Yatsuo around the EQ.1 earthquake in March 2022. The star symbol shows the time of the earthquake. (a) Comparison of data for 3 days around the day of the earthquake. Yellow highlighted periods are the same as in Figs. 4 and 5. (b) More detail on the day of the earthquake.

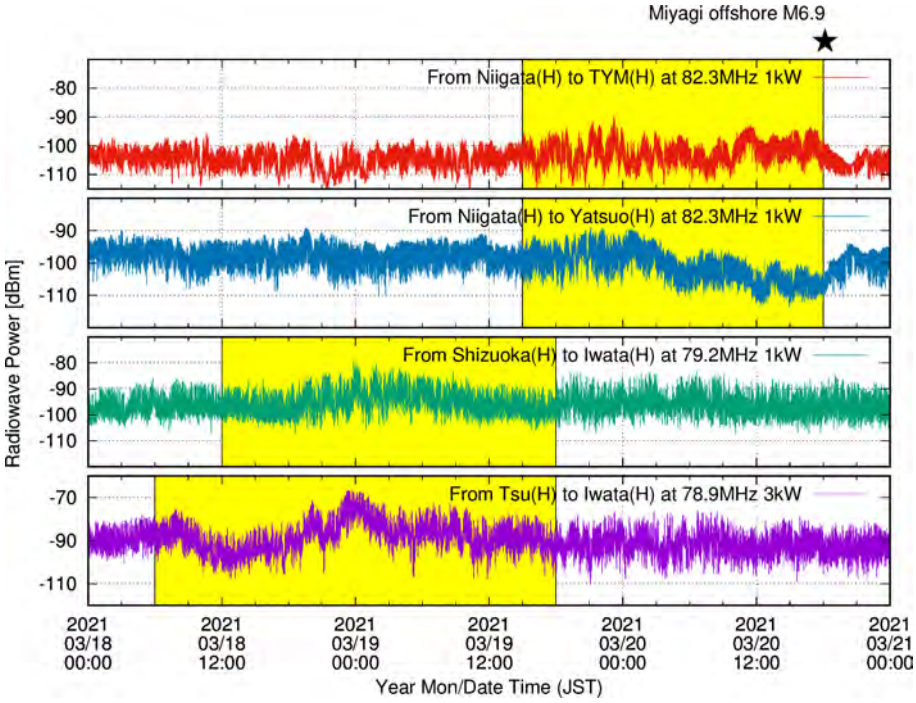


Figure 9: Expansion and comparison of the precursory signals observed in Iwata, Toyama, and Yatsuo around the EQ.2 earthquake in March 2021. The star symbol shows the time of the earthquake. Yellow-highlighted periods are the same as in Figs. 6 and 7.

### 3.2.3 Smaller Earthquakes and Their Precursors

The observed radio wave signal for EQ.3 Ibaraki offshore $M6.0$ earthquake on May 22, 2022, is shown in Figs. 10. For this event, the local seismic intensity observed in each region, where the Iwata observation station and the Toyama observation station are located, was 1 and 3, respectively. The rise time of the precursory signal on May 20, 2022, is much shorter than those of other earthquakes and this may be attributed to the much shallower epicenter at 5 km in depth than the others. In addition, a sudden drop is seen in 78.9 MHz data from Tsu on May 20 at approximately 5:00, which is a typical variation of such precursors.

For EQ.4 Ibaraki north $M5.4$ on Apr. 19, 2022, the observed radio wave signals are shown in Figs. 11. For this case, a clearer precursor is seen in Toyama than in Iwata (not shown). This may be because the epicenter is inland, not in the ocean, and closer to Toyama than Iwata as compared to the other earthquakes. The local seismic intensity observed in both regions of the Iwata and the Toyama observation station was 2.

For EQ.5 Ibaraki offshore $M5.3$ on May 29, 2022, the observed radio wave signal is shown in Figs. 12. For this event, the local seismic intensity observed in each region of the Iwata and the Toyama observation station was both 2. The epicenter is in the ocean closer to Iwata, for which the precursors may have been stronger in Iwata than in Toyama (not shown). For EQ.6 Ibaraki south $M4.8$ on May 5, 2022, the observed radio wave signals are shown in Figs. 13. Compared to the other examples of earthquakes, the rising part of the precursor is smaller and only the following rapidly fluctuating signals are seen. For those relatively small earthquakes, the precursory signals often delay; i.e., the precursory signals start simultaneously as the main shock and continue even after the event. Such delay could be because the underground crustal activity is small and occurs only concurrently with the main shock, while for larger earthquakes, there might be larger detectable crustal activity before the main shock.

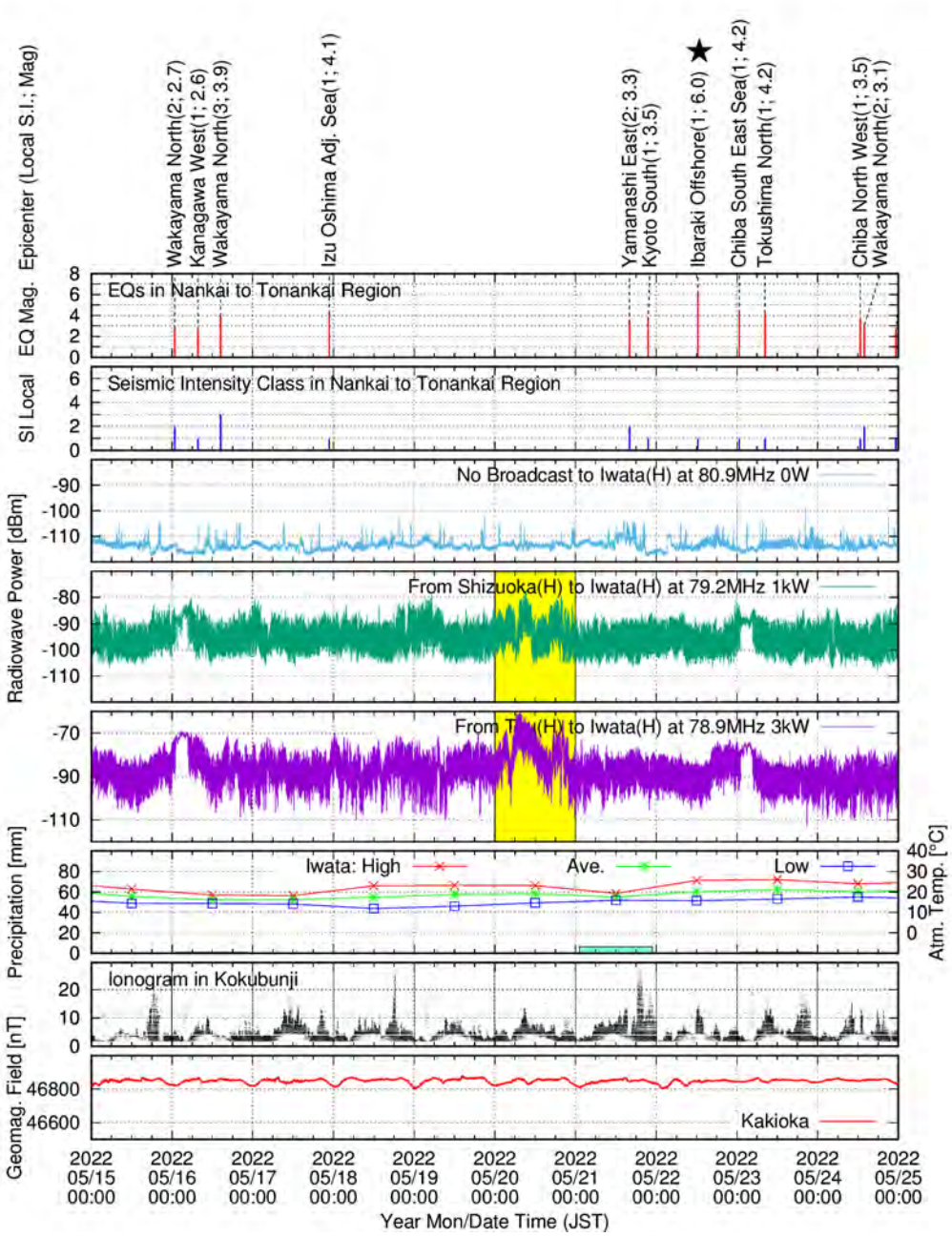


Figure 10: Observed radio wave power (dBm) at Iwata observation station on the Pacific side of Japan around EQ.3 Ibaraki offshore $M6.0$ on May 22, 2022, together with environmental data observed by national institutes. The main shock of EQ.3 is marked by a star.

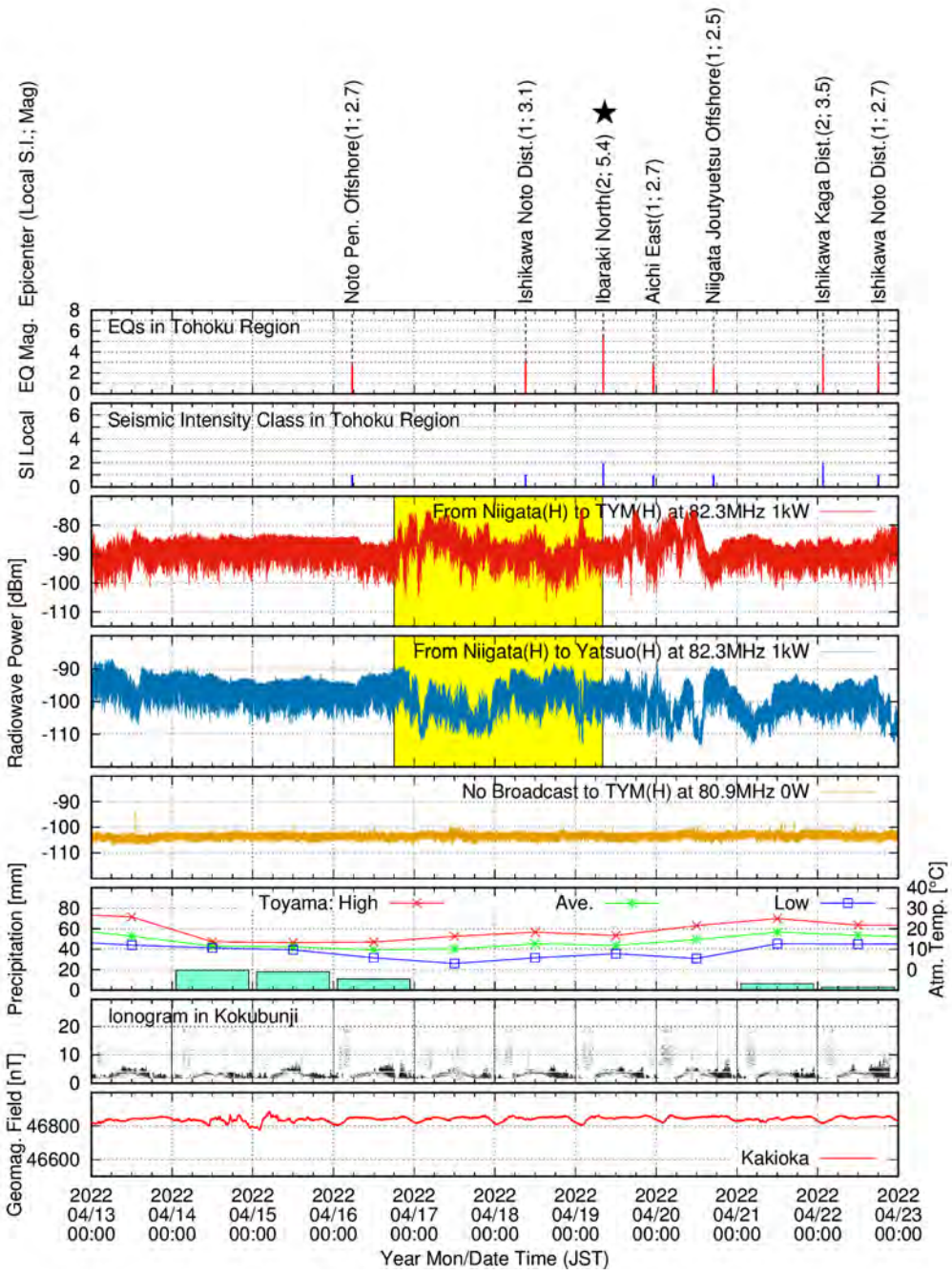


Figure 11: Observed radio wave power (dBm) at Toyama (TYM) and Yatsuo observation stations on the west side of Japan around EQ.4 Ibaraki north $M5.4$ on Apr. 19, 2022, together with environmental data observed by national institutes. The main shock of EQ.4 is marked by a star.

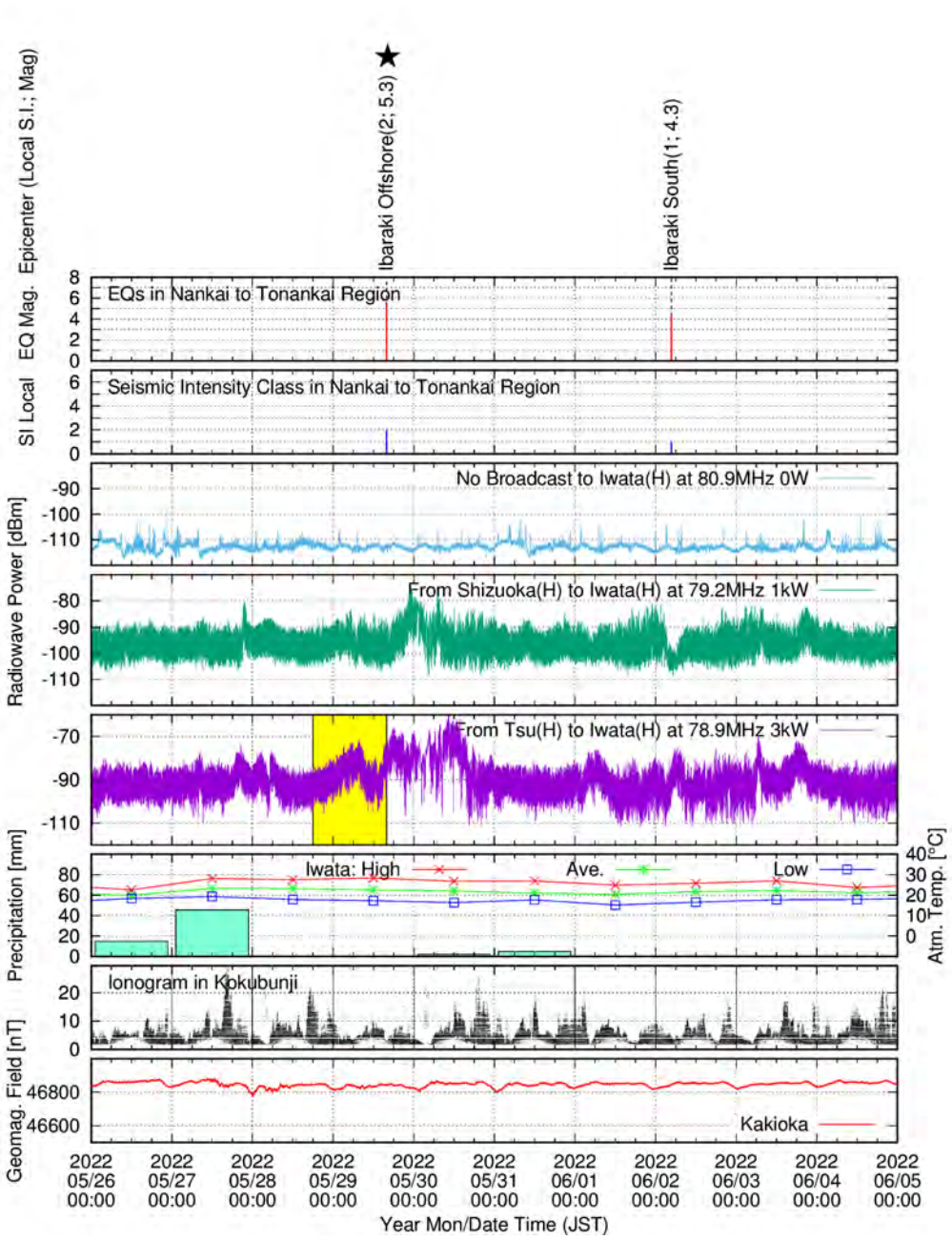


Figure 12: Observed radio wave power (dBm) at Iwata observation station on the Pacific side of Japan around EQ.5 Ibaraki offshore $M5.3$ on May 29, 2022, together with environmental data observed by national institutes. The main shock of EQ.5 is marked by a star.

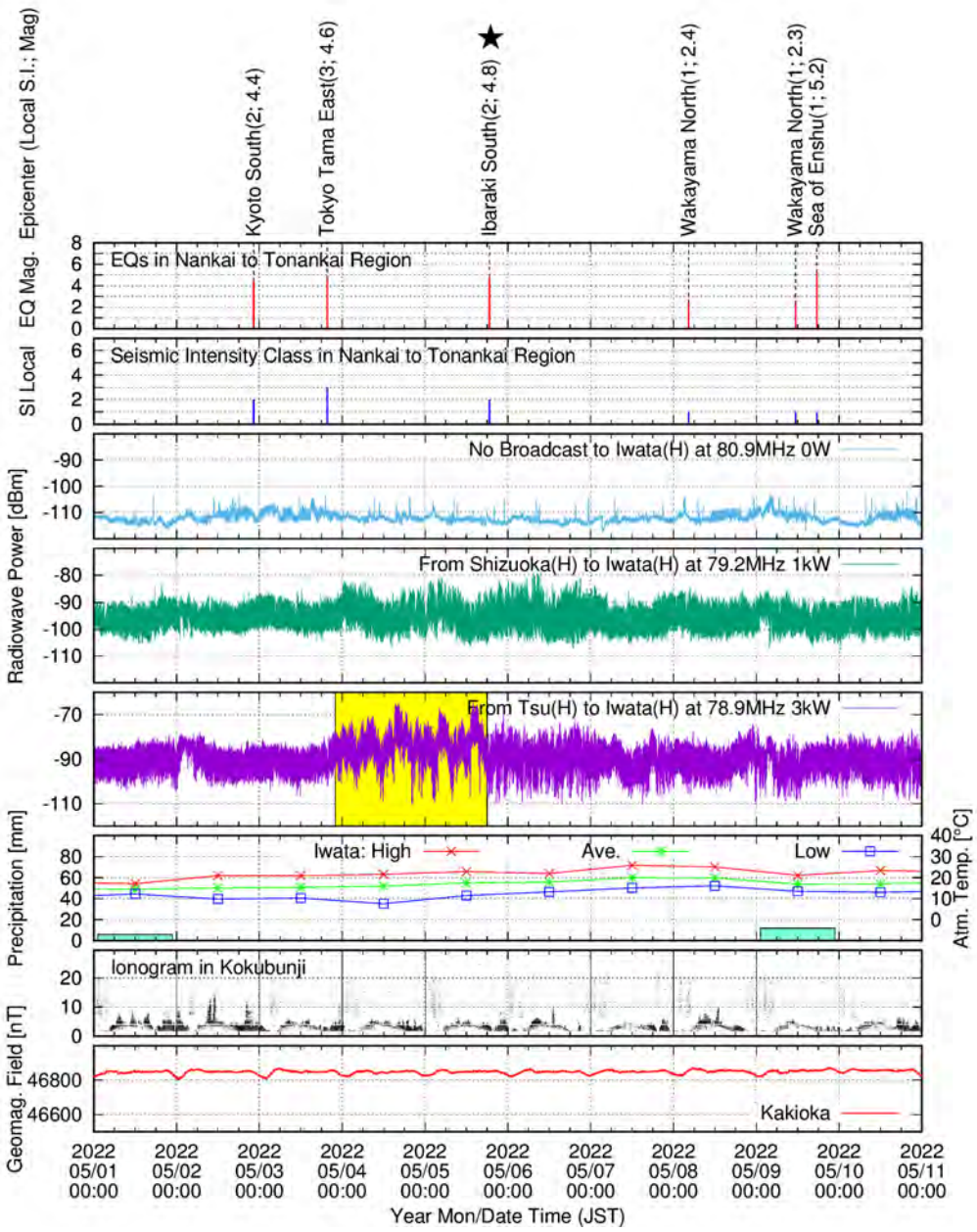


Figure 13: Observed radio wave power (dBm) at Iwata observation station on the Pacific side of Japan around EQ.6 Ibaraki south $M4.8$ on May 5, 2022, together with environmental data observed by national institutes. The main shock of EQ.6 is marked by a star.

## 3.3 Statistics and Probability between the Observed Electromagnetic Anomalies and Earthquake Occurrence

Electromagnetic precursors are detected reliably and steadily in some cases of the radio wave propagation in our observation. This provides us with chronological probability information about the impending earthquakes; i.e., whether an earthquake is about to occur shortly or will not occur for a while in a certain probability. The information on the location of the lithospheric stress and seismic activity would be obtained by placing more observation stations and considering the radio wave paths that may carry such precursors, and accumulating the data of precursors and earthquakes that happened. Although the strength of the precursory signals is often affected by meteorological conditions, larger earthquakes are expected to generate more electric charge carriers, leading to the precursors being detected more clearly at broader locations.

Although it is not possible to present all the data here, we have detected numerous precursors for many earthquakes. However, for relatively small earthquakes, the precursors are not necessarily always clear, and it often happens that the radio wave anomaly is oscillatory and confusing. Some earthquakes even occur without notable precursors, and some precursor-like signals are not associated with earthquakes. For example, the earthquake in Fukushima offshore $M7.3$ on February 13, 2021, at 23:07:50.5 JST, depth 55 km, Max S.I. 6+, did not exhibit precursors in Iwata observation station, but only at the Toyama observation station with similar precursors as of EQ.1 (not shown in this paper). The appearance and disappearance of the precursor is a subject of further research; the randomness of the precursor will be explained partly by the randomness of the interaction between the radio wave and the electrical charges on the ground surface, of which the shape and the electrical properties are particularly random. Their influence on the precursory phenomena has been studied by numerical analysis in the accompanying paper of Part II. The observation results in this paper show at least the possibility of detecting clear electromagnetic precursors of earthquakes. In this section, detailed statistics and probability analysis of the observed precursors are discussed.

### 3.3.1 Definition and Calculation of the Probabilities of Earthquake Prediction

The success rate of earthquake prediction $p$ is defined by

$$p = \frac{n_a}{N_a} \ , \tag{1}$$

where $n_a$ is the number of consecutive anomalous signals that successfully predicted the earthquakes, and $N_a$ is the total number of anomalous signals. This is the ratio of the anomalous radio wave signals that successfully predicted the occurrence of earthquakes within the effective period of the anomalous signal, which is defined as a period that starts from the beginning of the anomalous signal and ends at a time extended by $\tau$ after the end of the anomalous signal. We refer to the period of $\tau$ as the effective period of prediction, e.g., assuming $\tau = 3$ days in this paper, during which the anomalous signals are related to the earthquakes that follow.

Conversely, the earthquake predicted rate or the earthquake alarm rate, $q$ is defined by

$$q = \frac{n_p}{N_{eq}} \ , \tag{2}$$

where $n_p$ is the number of earthquakes that are successfully predicted by the anomalous signal, and $N_{eq}$ is the total number of earthquakes; this is the ratio of the earthquakes that are successfully predicted by the anomalous radio wave signals within the effective period $\tau$.

The prediction success rate $p$ and the earthquake predicted rate $q$ are in a contradictory relation; if the prediction is made in such a way that the number of predictions becomes too

large, then $q$ may increase but $p$ will decrease. If the prediction is made in such a way that the number of predictions becomes too small, then $p$ may increase but $q$ will decrease. Only if the prediction is made appropriately, i.e., the prediction by the anomalous signals is truly based on the precursors of earthquakes, both $p$ and $q$ become large. If $p$ is not large, the radio wave signals may contain irrelevant signals for more than the earthquakes detected in the district. Then, the district in which the earthquakes are searched for can be broadened. If $q$ is not large, the radio wave signals do not contain enough precursors that cover the earthquakes detected in the district, and the district in which the earthquakes are searched for can be narrowed.

The probability significance $\eta$, or sometimes referred to as probability gain, is given by the ratio between the prediction success rate $p$ to the random prediction success rate $p_0$ as

$$\eta = \frac{p}{p_0} \ , \tag{3}$$

where

$$p_0 = \frac{\tau}{\tau_0} \ , \tag{4}$$

and $\tau_0$ is the averaged interval of earthquakes; $\tau_0$ can be calculated as the total period of observation $T_{all}$ divided by the number of earthquakes that occurred during the period as

$$\tau_0 = \frac{T_{all}}{N_{eq}} \ . \tag{5}$$

which, however, may not represent the actual property of earthquakes if many earthquakes occur consecutively within a very short period. Such short intervals of earthquakes are omitted to find a more reasonable value of modified average interval $\tau_{0mod}$ of no earthquake occurrence as

$$\tau_{0mod} = \frac{\Sigma_{i=1}^{N_{intvl}} \tau_i}{N_{intvl}} \ , \tag{6}$$

where $\tau_i$ is the i-th interval larger than a certain period and $N_{intvl}$ the number of such intervals to be accumulated, each calculated from the actual list of earthquakes. Then, the modified probability significance $\eta_{mod}$ is given by

$$\eta_{mod} = \frac{p\,\tau_{0mod}}{\tau} \ . \tag{7}$$

### 3.3.2 Statistics and Probability Analysis Results

We have calculated the rates $p$ and $q$ for our observation results of Iwata - Tsu 78.9MHz radio wave; the list of earthquakes included in the analysis has been obtained from the JMA database of earthquakes [14] with the condition that Japan ' s seismic intensity index is larger than 1 within the district of Kanagawa, Shizuoka, Aichi, Mi-e, Nara, and Wakayama prefectures as shown by the red part in Fig. 14. Examples of the plots of chronological comparison between the anomalous signals and the earthquakes are those in Figs. 4, 6, 10, 12 and 13 for the Iwata observation signals.

The anomalous signals are judged empirically by the authors. The criteria for the judgement are (i) signal strength varies and abrupt rises and falls are observed, sometimes accompanied by fading-like noises; (ii) other influences from meteorological, ionospheric changes, or geomagnetic fields due to solar turbulences are not detected simultaneously, and independency from those effects is clear; and (iii) no changes in the 80.9 MHz signal level simultaneously, which can thus show the signal is not of broadband noises. It is noted that the amplitude of the anomalous

Figure 14: Map of the earthquake searching district for the probability analysis, i.e., Kanagawa, Shizuoka, Aichi, Mi-e, Nara, and Wakayama prefectures filled with red.

signals may vary seasonally, possibly due to the influence of atmospheric effects such as radio-ducting, albeit not a dominant effect. Taking into account the other radio wave signals of different frequencies will improve the accuracy of the judgment.

The period of the observation data analyzed here is from September 18, 2017, to July 27, 2022. The total number of days is 1,773. We observed a total of 348 anomalous signals including small and large ones. We assumed $\tau = 3$ days in the following analyses. To obtain the modified probability significance $\eta_{mod}$ (7), we omitted the intervals of earthquakes less than 12 hours, and calculating the nominal probability significance $\eta$ (3). The probabilities analyzed for the Iwata observation data are summarized in Table 2. If the probability significance $\eta$ or the modified probability significance $\eta_{mod}$ is larger than unity, i.e. $\eta, \eta_{mod} > 1$, $p$ and $q$ are statistically significant, $p$ and $q$ are insignificant for the case of $\eta, \eta_{mod} < 1$. $\eta$ and $\eta_{mod}$ are found to be similar for all the cases. Our results are thus statistically significant for $M = 4$, 5 and 6 of the seismic intensity of JMA (SI-JMA) $\geq 1$, and for all the cases of SI-JMA $\geq 2$.

For the statistically significant cases in Table 2, the prediction success rates $p$ are approximately 60 % and the earthquake predicted rates $q$ are 70 to 80 %. These probabilities larger than 50 % imply a possible strong correlation between the observed radio wave precursors and the earthquake occurrence. The prediction success rates $p$ are obviously worse for SI-JMA $\geq 2$ (Table 2(b)) than for SI-JMA $\geq 1$ (Table 2(a)), because the number of detected earthquakes is typically smaller for SI-JMA $\geq 2$. In contrast, the earthquake predicted rates are similar for both cases. This suggests that the radio wave precursors appear when the earthquake is as small as SI-JMA = 1 and $M2$. One of the reasons for the failure of prediction is that the effective period of prediction is $\tau = 3$ days but some large earthquakes occur after that period. Moreover, some earthquakes occur out of the search district of the earthquake database. For the particular cases of distant earthquakes in which the epicenter is farther than several hundred kilometers, anomalous signals are sometimes observed after the corresponding main shocks. Detailed probability analysis will be reported in our succeeding paper.

## 4 Conclusions

It has been shown that clear electromagnetic precursors are detected in VHF radio wave signals before Fukushima offshore $M7.4$ earthquake on March 16, 2022, by using high-sensitivity low-noise observation systems employing super-narrowband notch filters. Precursors have been

Table 2: Results of the probability analysis for the Iwata observation data and the earthquake occurrence searched in the district of Fig. 14.

(a) For the seismic intensity of JMA (SI-JMA) $\geq 1$. $p, q$ for the cases of $M4$, 5, 6 and larger are statistically significant.

| Magnitude | no. of EQs | $p$[%] | $q$[%] | $\eta$ | $\eta_{mod}$ |
|---|---|---|---|---|---|
| $M2$ and larger | 1025 | 92.0 | 73.0 | 0.53 | 0.74 |
| $M3$ and larger | 667 | 83.3 | 73.2 | 0.74 | 0.93 |
| $M4$ and larger | 285 | 59.5 | 80.7 | 1.23 | 1.38 |
| $M5$ and larger | 111 | 28.7 | 80.2 | 1.53 | 1.65 |
| $M6$ and larger | 29 | 7.8 | 82.8 | 1.58 | 1.63 |

(b) For SI-JMA $\geq 2$. $p, q$ are statistically significant for all the cases.

| Magnitude | no. of EQs | $p$[%] | $q$[%] | $\eta$ | $\eta_{mod}$ |
|---|---|---|---|---|---|
| $M2$ and larger | 381 | 64.9 | 76.4 | 1.01 | 1.22 |
| $M3$ and larger | 321 | 62.1 | 77.6 | 1.14 | 1.33 |
| $M4$ and larger | 178 | 42.8 | 80.9 | 1.42 | 1.52 |
| $M5$ and larger | 70 | 19.5 | 82.9 | 1.65 | 1.68 |
| $M6$ and larger | 20 | 5.5 | 85.0 | 1.61 | 1.65 |

detected consistently and steadily for various earthquakes from small to large events with the proposed observation systems. Typical precursory signals have been observed frequently on the radio wave path that crosses over large tectonic fault zones. We have detected similar and clear precursors at two distant locations for large earthquakes, which are considered to be the evidence of the precursors. In our observation data of approximately 5 years with statistical significance, more than 300 precursors are detected at our observation station on the pacific side, the prediction success rates $p$ of earthquakes $M3$ and larger are approximately 60 % and the earthquake predicted rates $q$ are 70 to 80 %. The location of the epicenter of earthquakes has not been predicted yet. It would be therefore expected to place more observation stations and accumulate the data of precursors. By comparing the precursor dataset with the earthquake database, valuable geographical knowledge might be extracted with high accuracy.

# 5 Open Research

Data of earthquakes from the searching service by the Japan Meteorological Agency (JMA) available at `https://www.data.jma.go.jp/svd/eqdb/data/shindo/index.html` [14]. Precipitation and temperature data from JMA at `https://www.data.jma.go.jp/obd/stats/etrn/` [16]. Ionograms from the National Institute of Communication Technologies (NICT), Japan at `https://wdc.nict.go.jp/cgi-bin/ionog/sum_control.cgi` [21]. Geomagnetic field data from JMA Kakioka Magnetic Observatory, 2013, Kakioka geomagnetic field 1-minute digital data in IAGA-2002 format [dataset], Kakioka Magnetic Observatory Digital Data Service, doi:10.48682/186bd.3f000, available at `http://www.kakioka-jma.go.jp/obsdata/metadata` [15].

Radio wave data and other environmental data integrated into synchronized diagrams by the author are available at `http://www3.u-toyama.ac.jp/densou01/RadiowaveDataPlots_5.5c_nohighlight/RadiowaveDataPlots_Shizuoka_Iwata_all.pdf` and `http://www3.u-toyama.ac.jp/densou01/RadiowaveDataPlots_5.5c_nohighlight/RadiowaveDataPlots_Toyama_Toyama_all.pdf`.

Figures were made with Gnuplot version 5.2.8 available under Copyright by T. Williams, and C. Kelley at `http://www.gnuplot.info` [30].

The map was created using Generic Mapping Tools (GMT) version 5.4.5, under Copyright by The GMT Developers (2019 - 2022) available at `https://www.generic-mapping-tools.org` [29].

## acknowledgments

This work is partly supported by the Japan Society for the Promotion of Science (JSPS) KAKENHI Grant Number 21K04059.

## References


[1] W. H. Bakun, B. Aagaard, B. Dost, W. L. Ellsworth, J. L. Hardebeck, R. A. Harris, C. Ji, M. J. S. Johnston, J. Langbein, and J. J. Lienkaemper. Implications for prediction and hazard assessment from the 2004 Parkfield earthquake. *Nature*, 437(13):969–974, Oct. 2005.

[2] T. Bleier, C. Dunson, S. Roth, J. Heraud, A. Lira, F. Freund, R. Dahlgren, R. Bambery, N. Bryant, J. Y. Liu, and G. Papadopoulos. *Earthquake Prediction Studies: Seismo Electromagnetics*, pages 1–15. Terrapub, 2013. Edited by M. Hayakawa.

[3] R. Dahlgren, M. Johnston, V. Vanderbilt, and R. Nakaba. Comparison of the stress-stimulated current of dry and fluid-saturated gabbro samples. *Bull. Seismo. Soc. Am.*, 104(6):2662–2672, Dec. 2014.

[4] Y. Enomoto and H. Hashimoto. Emission of charged particles from indentation fracture of rocks. *Nature*, 346:641–643, Aug. 1990.

[5] F. Freund. Time-resolved study of charge generation and propagation in igneous rocks. *J. Geophysical Res., Solid Earth*, 105(B5):11001–11019, 2000.

[6] F. Freund. Pre-earthquake signals: underlying physical processes. *J. of Asian Earth Sciences*, 41:383–400, 2011.

[7] F. Freund. Earthquake forewarning - a multidisciplinary challenge from the ground up to space. *Acta Geophysica*, 61(4):775–807, Aug. 2013.

[8] M. Fujii. Theory of ground surface plasma wave associated with pre-earthquake electrical charges. *Radio Science*, 48:122–130, Mar. 2013.

[9] M. Fujii. Fundamental correction of Mie's scattering theory for the analysis of plasmonic resonance of a metal nanosphere. *Phys. Rev. A*, 89(3):033805, Mar. 2014.

[10] M. Fujii. A new mode of radio wave diffraction via the terrestrial surface plasmon on mountain range. *Radio Science*, 51:1396–1412, Aug. 2016.

[11] M. Fujii. Notch filter, Japan patent 6846789, 2021.

[12] H. Fujiwara, M. Kamogawa, M. Ikeda, J. Y. Liu, H. Sakata, Y. I. Chen, H. Ofuruton, S. Muramatsu, Y. J. Chuo, and Y. H. Ohtsuki. Atmospheric anomalies observed during earthquake occurrences. *Geophys. Res. Lett.*, 31:L17110, 2004.

[13] M. Hayakawa, V. V. Surkov, Y. Fukumoto, and N. Yonaiguchi. Characteristics of VHF over-horizon signals possibly related to impending earthquakes and a mechanism of seismo-atmospheric perturbations. *J. of Atmospheric and Solar-Terrestrial Phys.*, 69:1057–1062, 2007.

[14] JMA-EQ. Japan meteorological agency seismic intensity database search.

[15] JMA-GM. Geomagnetic digital data service.

[16] JMA-Weather. Japan meteorological agency previous weather data search.

[17] C. Kittel. *Introduction to solid state physics*. John Wiley and Sons, Inc., New York, 6th edition, 1986.

[18] Y. Kushida. *Earthquake Forcast*. PHP Shinsho, Tokyo, 2012. in Japanese.

[19] T. Moriya, T. Mogi, and M. Takada. Anomalous pre-seismic transmission of VHF-band radio waves resulting from large earthquakes, and its statistical relationship to magnitude of impending earthquakes. *Geophysical J. Int.*, 180:858–870, 2010.

[20] T. Nagao, Y. Enomoto, Y. Fujinawa, M. Hata, M. Hayakawa, Q. Huang, J. Izutsu, Y. Kushida, K. Maeda, K. Oike, S. Uyeda, and T. Yoshino. Electromagnetic anomalies associated with 1995 Kobe earthquake. *J. Geodynamics*, 33:401–411, 2002.

[21] NICT. Ionosheric sounding data in japan, ionogram.

[22] H. Raether. *Surface Plasma Oscillations and Their Applications*, volume 9 of *Physics of Thin Films*, pages 145–261. Academic Press, New York, 1977.

[23] H. Raether. *Surface plasmons on smooth and rough surfaces and on gratings*. Springer-Verlag, Berlin, 1988. p.5.

[24] T. Rikitake and Y. Yamazaki. Precursory and coseismic changes in ground resistivity. In *Earthquake Precursors, Proceedings of the US-Japan Seminar on Theoretical and Experimental Investigations of Earthquake Precursors*, pages 161–173, Tokyo, 1978.

[25] J. Scoville, J. Sornette, and F. Freund. Paradox of peroxy defects and positive holes in rocks Part II: Outflow of electric currents from stressed rocks. *J. of Asian Earth Sciences*, 114-2:338–351, Dec. 2015.

[26] A. Takeuchi and T. Nagao. Activation of hole charge carriers and generation of electromotive force in gabbro blocks subjected to nonuniform loading. *J. Geophysical Res., Solid Earth*, 118:915–925, 2013.

[27] S. Uyeda, T. Nagao, Y. Orihara, T. Yamaguchi, and I. Takahashi. Geoelectric potential changes: Possible precursors to earthquakes in japan. *PNAS*, 97(9):4561–4566, 2000.

[28] P. Varotsos and K. Alexopoulos. Physical properties of the variations of the electric field of the earth preceding earthquakes, i. *Tectonophysics*, 110:73–98, 1984.

[29] P. Wessel. The generic mapping tools.

[30] T. Williams and C. Kelley. Gnuplot homepage.